Radiative cooling of polyyne anions: C_4H^- and C_6H^-

Boxing Zhu,[1] James N. Bull,[2] José Navarro Navarrete,[1] Alice Schmidt-May,[1] Henrik Cederquist,[1] Henning T. Schmidt,[1] Henning Zettergren,[1] and Mark H. Stockett[1, a)]

[1)] *Department of Physics, Stockholm University, SE-10691 Stockholm, Sweden*

[2)] *School of Chemistry, Norwich Research Park, University of East Anglia, Norwich NR4 7TJ, United Kingdom*

(Dated: 3 October 2022)

Time-dependent photodetachment action spectra for the linear hydrocarbon anions C_4H^- and C_6H^- are investigated using the cryogenic electrostatic ion storage ring DESIREE. Radiative cooling characteristics of the ions on the millisecond to seconds timescale are characterized by monitoring changes in the spectra as the ions cool by spontaneous infrared (IR) emission. The average cooling rates, extracted using Non-negative Matrix Factorization, are fit with $1/e$ lifetimes of 19 ± 2 s and 3.0 ± 0.2 s for C_4H^- and C_6H^-, respectively. The cooling rates are successfully reproduced using a simple harmonic cascade model of IR emission. The ultraslow radiative cooling dynamics determined in this work provide important data for understanding the thermal cooling properties of linear hydrocarbon anions and for refining models of the formation and destruction mechanisms of these anions in astrochemical environments.

I. INTRODUCTION

As important intermediates in the initial stage of Polycyclic Aromatic Hydrocarbons formation, the linear carbon monohydride radical chains are of great astrochemical significance.[1] The chemical growth of carbon chains has been studied for some decades, with two main growth hypotheses based on top-down and bottom-up mechanisms involving charged molecules.[2] Low energy ion-neutral reactions are considered as the main class of reaction responsible for most interstellar chemical synthesis. Although the formation of small negatively charged species, including H^-, has been proposed for decades,[3,4] it was not until the first carbon chain anion C_6H^- was detected in the interstellar medium (ISM) more than a decade ago that interest in anions was rekindled.[5] It is remarkable that the column density of C_6H^- is surprisingly high at 1–5% of that for neutral C_6H.[5] Subsequently, C_4H^-,[6] C_8H^-,[7] CN^-,[8] C_3N^-,[9] and C_5N^-,[10] have been identified in the ISM. While around 220 molecules and 32 cations have been detected in the ISM or circumstellar shells, studies of anions in astrochemical contexts have been sparse.

In recent years, the discovery of anions and their incorporation into chemical models have increased the need to better understand their formation and destruction dynamics. In particular, some molecules have been observed in vastly different concentrations compared to predictions, indicating that the present astrochemical models need refinement, possibly considering anion abundance and photo-processing.[11–13] Key information required for these models include vibrational radiative emission rates,[12,14] which is a property difficult to measure in conventional laboratory experiments. Furthermore, anions in space have been postulated to be carriers of some diffuse interstellar bands (DIBs). For example, the $A^1B_1 \leftarrow X^1A'$ excitation into the dipole-bound state of the cyanomethyl anion CH_2CN^- has strong relationship with the $\lambda 8040$ DIB.[15–17]

This contribution reports on the radiative cooling lifetimes for C_4H^- and C_6H^- using the cryogenic electrostatic ion storage ring DESIREE.[18] The near collision-free ($\approx 10^{-12}$ Torr) and low-temperature ($T \approx 10$ K) conditions available in DESIREE provide an environment resembling that of cold molecular clouds. Action spectroscopy experiments on astrochemically relevant ions in electrostatic ion storage devices are important because they give access to slow processes such as unimolecular dissociation and statistical vibrational autodetachment (thermionic emission),[19–21] which occur on timescales up to hundreds of milliseconds, and also ultraslow processes including IR radiative cooling, which may proceed over hundreds of seconds.[22–24] Here, the radiative cooling of C_4H^- and C_6H^- is probed using two-dimensional (*i.e.* storage time and excitation wavelength dependent) photodetachment action spectroscopy as a hot ensemble of stored ions cool. The time-dependent contribution of hot bands to the action spectrum is extracted using Non-negative Matrix Factorization (NMF), quantifying the progress of vibrational cooling. IR radiative cooling characteristics for C_4H^- and C_6H^- are compared with predictions from a simple harmonic cascade (SHC) model. The adiabatic detachment energy (ADE) for C_4H^- obtained from the NMF-analyzed cold-ion spectrum is in good agreement with literature determinations.

II. METHODS

A. Experiments

The DESIREE (Double ElectroStatic Ion Ring ExpEriment) storage ring facility is located at the Department of Physics, Stockholm University, and has been described previously.[18] In the present experiment, we used the symmetric storage ring illustrated in FIG. 1 that has a circumference of 8.7 m. The multilayer insulated DESIREE vacuum chamber and the ion guiding electrostatic deflectors and detectors are cooled to $T \approx 13$ K by helium refrigerators. The entire system is kept at vacuum of $\approx 10^{-12}$ Torr with a residual gas density on the order of $\sim 10^4$ cm^{-3} (consisting mainly of

[a)] Electronic mail: mark.stockett@fysik.su.se

H_2), providing a nearly collision-free environment and allowing keV ion beams to be stored for times exceeding hundreds of seconds.[25,26]

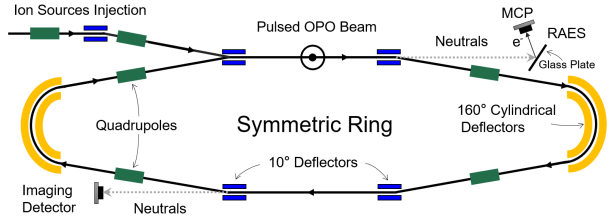

FIG. 1. Schematic drawing of the DESIREE ion storage ring. The OPO laser beam intersects perpendicularly with the ion beam on the RAES detector side. Neutral products formed through photodetachment along the straight section are detected by the glass plate and microchannel plate (MCP) detector.

Beams of $C_{2n}H^-$ (n = 2, 3) ions were produced using a cesium sputtering ion source (National Electrostatics Corp., Madison, Wisconsin) with a ^{13}C-enriched graphite cathode, where sputtered carbon clusters react with residual water in the source to form hydrocarbons.[18] Isotopic ^{13}C is an important consideration for ensuring that the pure isotopologues $^{13}C_{2n}H^-$ without contamination from pure carbon clusters (see further details in the Supplemental Information). The C_4H^- and C_6H^- species studied in this work are the isotopologues $^{13}C_4H^-$ and $^{13}C_6H^-$, respectively. Ions formed in the source are accelerated to 15 keV and injected into the symmetric storage ring. The ion-beam storage lifetime is typically >200 s, determined by laser probing (330 nm) the stored ion over a 550 s storage cycle.

For the action spectroscopy experiments, a tunable-wavelength OPO laser system (EKSPLA NT242, 1 kHz frequency) was used to excite the target ions in a crossed-beam geometry. Neutral particles formed through photodetachment or photodissociation in the straight section continue to travel at high speed (2.3×10^5 m s^{-1} for C_4H^-) until they strike a graphene-coated glass plate as part of the detector. Secondary electron ejection induced by neutral particle impacts on the glass plate are detected by a triple-stack microchannel plate (MCP) with a resistive anode encoder (RAE). The detector was gated with a 1 μs duration pulse slightly delayed with respect to the time of laser irradiation of the ions, eliminating scattered laser light signal. Photodetachment signals were generated by irradiating the stored ions every 1 ms (1 kHz repetition rate of laser) at a given OPO wavelength for a given ion storage time (0–55 s). The 2D photodetachment spectrum for a given anion was constructed from the time-dependent photodetachment signals with the OPO wavelength stepped between injections.

The 2D photodetachment action spectra were analyzed using Non-negative Matrix Factorization (NMF),[27,28] which are set of algorithms for dimensionality reduction, source separation, and topic extraction. NMF is a multivariate analysis and linear algebra algorithm designed to extract non-negative signatures and relative contributions of pure components from an additive mixture of those components. The present 2D spectra involve several components (e.g. hot and cold spectra) with distinct decay properties; NMF can separate these components and provide the time evolution of the components. NMF decomposition involves additive combinations of latent factors and requires that all elements in the data matrix $\mathbf{X}$ are non-negative. The matrix $\mathbf{X}$ is assumed to be the product of two non-negative matrices: the latent factors $\mathbf{H}$ and their corresponding weights $\mathbf{W}$ *i.e.* $\mathbf{X}$=$\mathbf{WH}$. The algorithm minimizes the divergence $\| \mathbf{X}\text{-}\mathbf{HW} \|_F$, subject to the constraints $\mathbf{H} \geq 0$, $\mathbf{W} \geq 0$. For our data sets, $\mathbf{X}$ represent a $\mathbf{m} \times \mathbf{n}$ matrix of photodetachment spectra, where $\mathbf{m}$ is the number of measured wavelengths and $\mathbf{n}$ is the number of storage-time bins. Using NMF, the radiative cooling rate and the cold-ion photodetachment spectrum can be extracted from the 2D action spectrum.

Compared to principal component analysis (see Supplemental Information), which was used for similar analysis in earlier studies,[24,29,30] the latent components obtained through NMF are more readily interpreted, and the non-negativity constraint is consistent with the physical requirement that the photodetachment yield is non-negative. **NMF factors are colinear while principal component analysis (PCA) components are orthogonal which means that PCA components are dependent on the preceding and variation. PCA is likely to give negative results, mainly because PCA is sensitive to outliers in the data that produce large errors, which the method tries to avoid in the first place. For example, in the current experiment, the PCA analysis gave a large error due to the presence of some long-lived states near the detachment threshold of $C_{2n}H^-$ (n = 2, 3) anions.**

B. Adiabatic detachment energies

According to the Wigner threshold law,[31,32] the adiabatic detachment energy (ADE) E_a for anions can be extracted from the following rule:

$$\sigma_{PD} = A(E_{ph} - E_a)^{\alpha} + B, \tag{1}$$

where σ_{PD} is photodetachment cross section, A and B are constants, E_{ph} and E_a are the photodetachment and adiabatic detachment energy, respectively, and α is the exponential factor. We tried to use this expression resembling the Wigner law for atomic anion thresholds to extract the photodetachment threshold. We found that the data fits best if the exponent α = 5/2.

C. Radiative cooling lifetime modeling

Spontaneous radiative cooling was analyzed using a simple harmonic cascade (SHC) model, which has been described in recent publications[24,33] with the following equation:[19]

$$k_s(E) = A_s^{10} \sum_{\upsilon_s=1}^{\upsilon_s \leq E/h\nu_s} \frac{\rho(E - \upsilon_s h\nu_s)}{\rho(E)}, \tag{2}$$

where E is the energy of a given vibrational state, h is Planck's constant, and the summation is over υ_s (υ_s = 0 and $\upsilon_s \geqslant 1$

are the quantum numbers of the vibrational ground and excited states for the mode ν_s). The density of vibrational states $\rho(E)$ was calculated using the Beyer–Swinehart algorithm with scaled harmonic vibrational mode frequencies ν_s.[24,34] The SHC model assumes that the only allowed emissions are those where $\Delta\upsilon_s$ = -1. The Einstein coefficients A_s^{10} and the harmonic vibrational frequencies were calculated at the B3LYP//6-311++G(2d,p) level of density functional theory in Gaussian 16.[35,36]

The SHC model starts from a Boltzmann distribution of vibrational energies of a hot molecular ensemble and simulates the temporal evolution of internal energies with ion storage time. The initial population density $g(E,t = 0)$ can be described as:

$$g(E,t=0) = (\rho(E) * e^{-E/(k_B T)})/(\sum_E \rho(E) * e^{-E/(k_B T)}), \quad (3)$$

where k_B is Boltzmann constant and T is the temperature determining the initial vibrational energy distribution. Radiative cooling processes are the time evolution of the internal energy distribution, given by:

$$\begin{aligned} g(E,t+dt) &= \sum_s g(E,t) e^{-k_s(E)dt} \\ &+ \sum_s g(E+h\nu_s,t)(1-e^{-k_s(E+h\nu_s)dt}). \end{aligned} \quad (4)$$

where the total energy remaining in the ensemble as a function of time, $E_{tot}(t) = \int E g(E,t) dE$, was taken as an indicator of the progress of cooling.

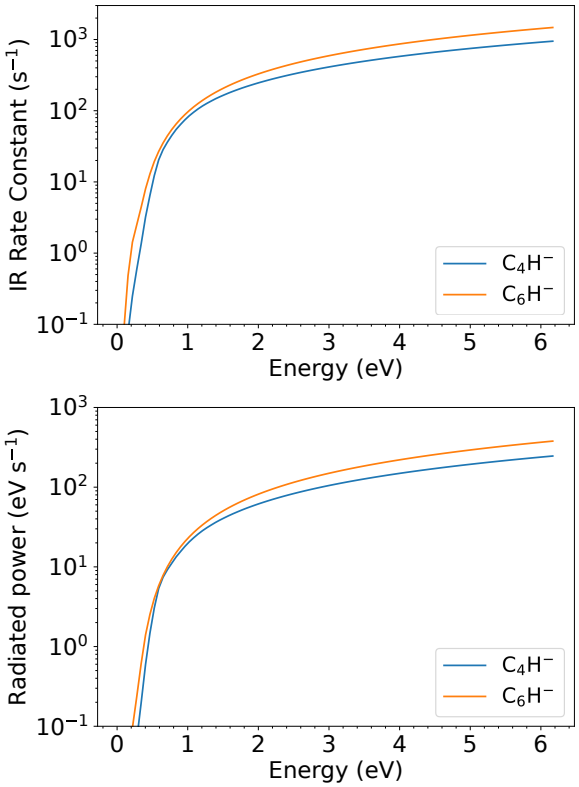

FIG. 2. Upper panel: The radiative cooling rate (k_{tot}) for C_4H^- and C_6H^- (note the log scale). Lower panel: The radiated power (p_{tot}) for C_4H^- and C_6H^- (note the log scale).

III. RESULTS AND DISCUSSION

A. Radiative rate

The total radiative cooling rate (k_{tot}) given in the upper panel of FIG. 2 was calculated by sum of radiative cooling rates for all vibrational modes $k_{tot}(E) = \sum_s k_s(E)$. The radiative power ($p_{tot}$) in the lower panel of FIG. 2 was calculated by the formula $p_{tot}(E) = \sum_s h\nu_s k_s(E)$. In FIG. 3, when starting from an initial Boltzmann distribution of vibrational energy corresponding to $T = 100$ K, the population density for C_4H^- and C_6H^- was calculated according to Equation 3. The radiative rate calculated with the SHC model shows a sharp decrease at low internal energy for both C_4H^- and C_6H^-. In accord with the vibrational energy distribution, the radiative cooling rate of C_6H^- is more rapid than for C_4H^-, consistent with an increase of the radiation rate with the number of IR active vibrational degrees of freedom.

B. C_4H^-

A photodetachment spectrum to survey the 330–375 nm range (2.5 nm steps) for C_4H^- as a function of ion storage time (up to 55 s) is shown in FIG. 4. Time-binned spectra (relative to ion injection) are shown in FIG. 5, providing insight into the photodetachment spectrum's evolution as the ions cool. Single exponential decay fits to the photodetachment signal with ion storage time at several selected probe wavelengths are presented in FIG. S5 (Supplemental Information), giving $1/e$ lifetimes ranging from 49 ± 11 s (330 nm) to 10 ± 2 s (360 nm). No significant time evolution was observed at longer wavelengths. The trend that hot-band contributions at longer wavelengths decay more rapidly is consistent with measurements on carbon cluster anions.[24]

The 2D photodetachment spectrum for C_4H^- was analyzed by NMF using two latent components: $\mathbf{H}_1$ and $\mathbf{H}_2$. Comparing these components to the time-binned spectra (see FIG. 5), we identify $\mathbf{H}_1$ with the cold-ion photodetachment spectrum, and $\mathbf{H}_2$ with all hot-band contributions associated with detachment from vibrationally excited states. The cold-ion spectrum $\mathbf{H}_1$ resembles the 30–55 s time-binned photodetachment spectrum, demonstrating that NMF is suitable for decomposing the 2D photodetachment spectrum. A single-exponential fit of $\mathbf{W}_2$, the weight of the $\mathbf{H}_2$ hot-band component (see FIG. 6), provides a lifetime of 19 ± 2 s, which should be considered as an averaged cooling lifetime across the selected wavelength range. The SHC model was used to interpret the IR radiative cooling characteristic $\mathbf{W}_2$. In FIG. 6, $\mathbf{W}_2$ with ion storage time is shown and was fit with a lifetime of 25.05 ± 0.05 s. SHC simulation of IR cooling is shown in FIG. 6, which was

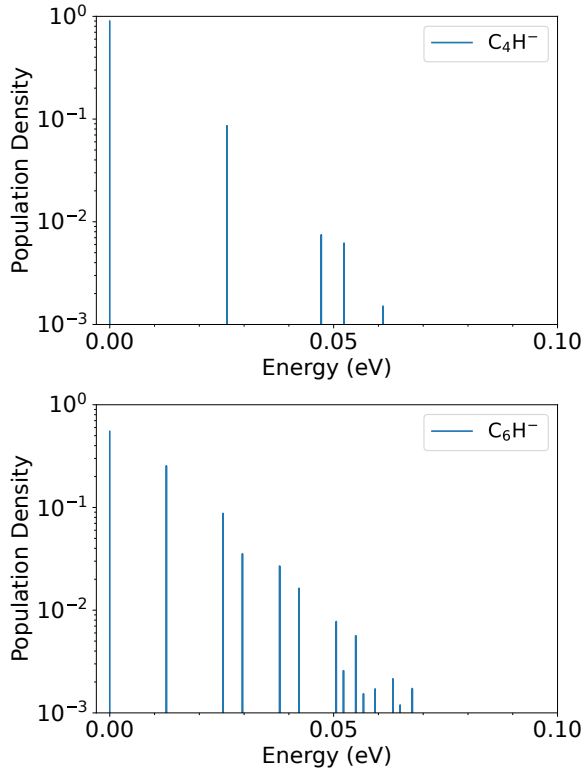

FIG. 3. Vibrational energy distribution for C_4H^- and C_6H^- at $T = 100\pm$ K (note the log scale).

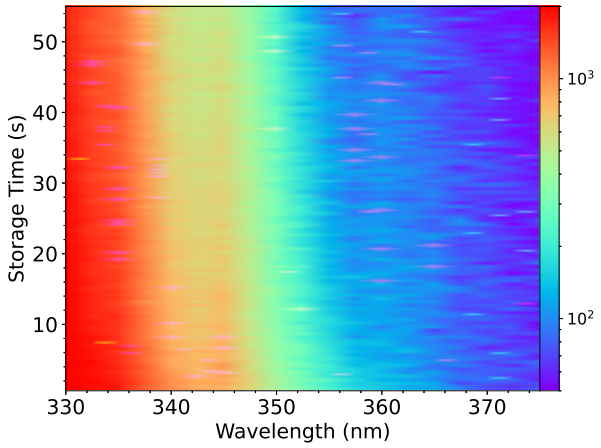

FIG. 4. 2D photodetachment spectrum for C_4H^-. The intensity of the photodetachment action spectrum is given by the log color scale.

optimized by adjusting the initial temperature (100 ± 10 K). The simulated cooling rate deviates from experiment by about 30%, which is typical for the SHC model.[24] Simulations assuming higher vibrational temperatures produced cooling dynamics too rapid compared with experiment.

For C_4H^-, both the 40–55 s time-binned photodetachment spectrum and the NMF-extracted cold-ion spectrum $\mathbf{H}_1$ were fit with the Wigner threshold law, giving ADE values of 3.40

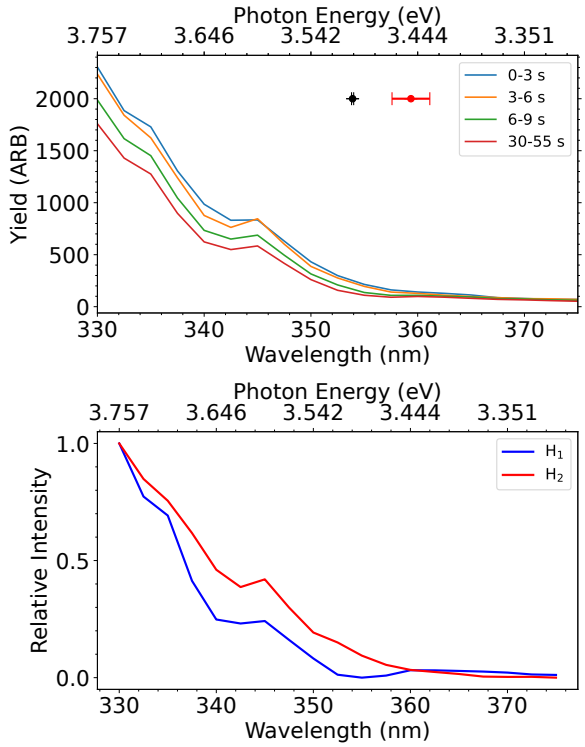

FIG. 5. Upper panel: Time-binned photodetachment spectra for C_4H^- in different time slices. The data markers represent the ADE (red value from $\mathbf{H}_1$ and black value from Ref. 37). Lower panel: Latent components from NMF analysis. The intensities of both components are normalized.

± 0.02 eV (365 ± 2 nm) and 3.45 ± 0.02 eV (359 ± 2 nm), respectively, which are lower than jet-cooled photoelectron spectroscopy data (3.533 ± 0.001 eV).[37,38] The discrepancy is likely due to contributions from hot bands that have not completely relaxed within 55 s.

A higher-resolution 2D photodetachment spectrum for C_4H^- over the first 5 s of cooling was measured over the 330–375 nm range. From the time-binned spectra and NMF analysis, the photodetachment spectrum exhibits no secular time dependence over the first 5 s cooling (see FIG. S1–S3 in supplementary materials). Comparison of the photodetachment spectrum from the 4–5 s time bin and the $\mathbf{H}_1$ for 55 s storage-time experiment shows that hot band contributions are still significant after 5 s (see FIG. S6).

C. C_6H^-

The 2D photodetachment spectrum for C_6H^- was recorded in 0.5 nm increments for the 315–360 nm range up to 5 s storage time (see FIG. 7). Time-binned spectra are shown in FIG. 8. In contrast to the relatively smooth photodetachment spectrum of C_4H^-, several resonances are seen for C_6H^-. Six selected probe wavelengths of the photodetachment signal decay are shown in FIG. S9, which were fit with single-

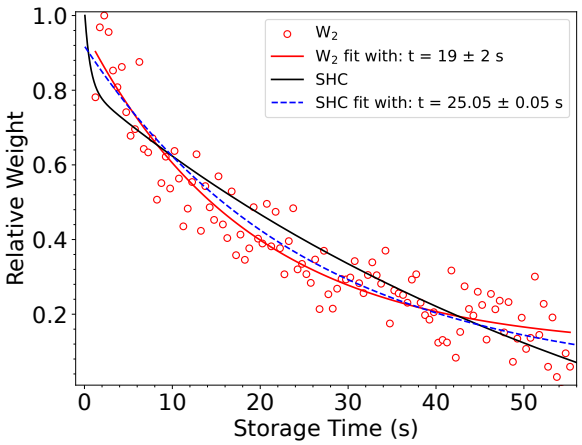

FIG. 6. Relative weight $\mathbf{W}_2$ of the hot component $\mathbf{H}_2$ with ion storage time, and relative total internal energy (E_{tot}) from the SHC radiative cooling model for C_4H^- (same axis scale).

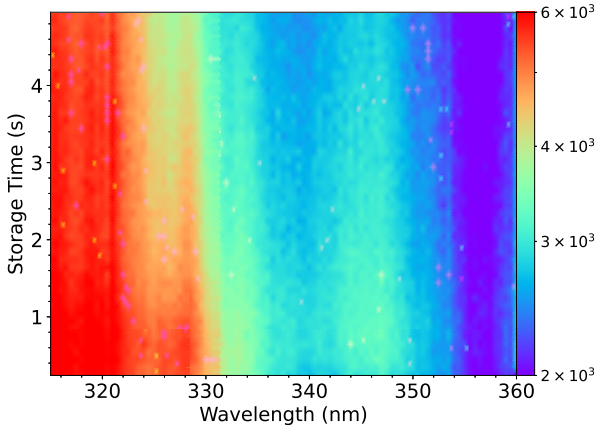

FIG. 7. 2D photodetachment spectrum for C_6H^-. The intensity of the photodetachment action spectrum is given by the log color scale.

exponential decays.

The 2D photodetachment spectrum for C_6H^- was interpreted using the NMF method using two latent components: $\mathbf{H}_1$ and $\mathbf{H}_2$ (see FIG. 8). Analysis from the corresponding weights of the $\mathbf{H}$ components indicates that $\mathbf{H}_1$ is a rapidly decaying component while the $\mathbf{H}_2$ shows no secular time dependence. An exponential fit to the $\mathbf{W}_1$ component with storage time (FIG. 9) gave the average cooling lifetime of 3.0 ± 0.2 s. SHC modeling of IR cooling reproduced the experimental trend gave a fitted lifetime of 2.448 ± 0.003 s, which is in good agreement with experiment.

As a final comparison, the NMF-extracted photodetachment spectra for C_6H^- are compared with a jet-cooled photodetachment spectrum recorded using a similar OPO laser system ($T \approx 50$ K, see Ref. 41 for experimental details) in FIG. 10. In agreement with high-resolution photodetachment spectra,[42] signatures in the jet-cooled spectrum are evident for several valence-bound states (VBS) and a dipole-bound state (DBS) through resonant-enhanced multi-photon detachment. Spectroscopic assignment of these features is summarized in Ref. 42. Briefly, a DBS is a non-valence state in which the excess electron is weakly bound (several tens of millielectron volts) at the positive end of the dipole moment associated with the neutral core.[43] Comparison of the NMF spectra with the jet-cooled spectrum shows that the $^1\Pi$ elec-

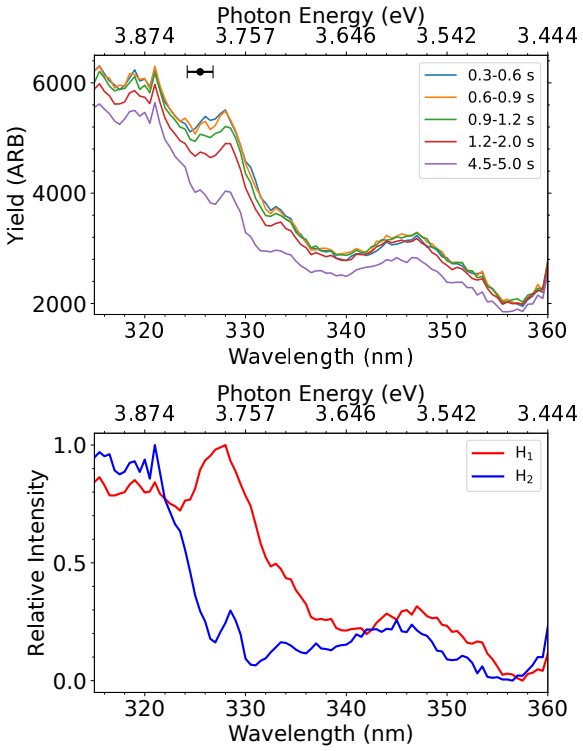

FIG. 8. Upper panel: Time-binned photodetachment spectra for C_6H^- in different timeslots. The data markers indicate the ADE and uncertainty (black value from Ref. 39). Lower panel: Main components from NMF analysis. The intensity of both components are normalized.

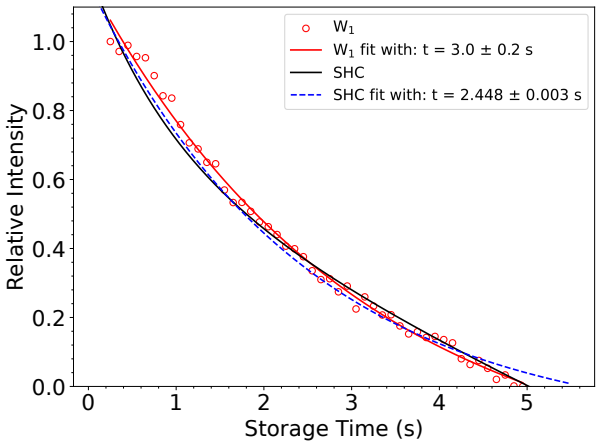

FIG. 9. Relative weight $\mathbf{W}_1$ of the hot component $\mathbf{H}_1$ with ion storage time, and relative total internal energy (E_{tot}) from the SHC radiative cooling model for C_6H^- (same axis scale).

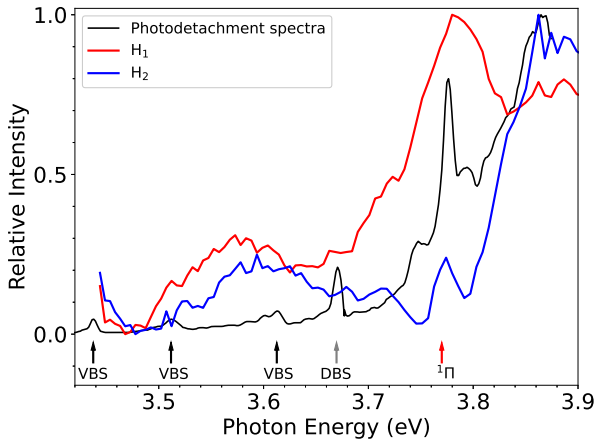

FIG. 10. Comparison of the NMF-etracted photodetachment spectra with a jet-cooled photodetachment spectrum[40] for C_6H^-. VBS is valence-bound state and DBS is dipole-bound state.

tronic state[42] marked with red arrow is evident in all cases, although the VBS and DBS present as a broad distribution in the NMF components presumably because of high rotational temperatures.[44]

IV. SUMMARY

The infrared radiative cooling lifetimes of two astrochemically relevant anions, C_4H^- and C_6H^-, have been investigated under collision-free conditions in a cryogenic ion storage ring using 2D photodetachment action spectroscopy. Time dependent hot-band components and cold-ion photodetachment spectra were separated by Non-negative Matrix Factorization to analyze the IR radiative cooling rates. Average cooling lifetimes are 19 $\pm$ 2 s for C_4H^- and 3.0 $\pm$ 0.2 s for C_6H^-. IR radiative cooling rates have been simulated using a Simple Harmonic Cascade model in good agreement with experiment. The ADE for C_4H^- obtained from the NMF-extracted cold-ion spectrum is consistent with earlier jet-cooled data, confirming that NMF is able to extract meaningful spectra associated with vibrationally-cold ions.

In the context of interstellar anion formation, the radiative electron attachment and dissociative electron attachment of a precursor (neutral) carbene are the most likely formation mechanisms for the polyyne anions.[45] The present experiments have shown the ability for hot C_4H^- and C_6H^- radiatively cool through IR emissions, providing lifetimes that can be incorporated into astrochemical models to predict column densities in the ISM or circumstellar shells. Significantly, the finding that the radiative cooling rate for C_6H^- is higher than that for C_4H^- is consistent with an increase of the radiative attachment rate with the number of IR active vibrational degrees of freedom.

V. SUPPLEMENTARY MATERIAL

The Supporting Information is available free of charge on the AIP Publications website.

Additional experimental data, SHC modeling deduced IR rate constants and computational results are present in the Supplementary Material. (PDF)

ACKNOWLEDGMENTS

The authors wish to acknowledge the support of the Swedish Research Council (grant numbers 2016-03675, 2016-04181, 2020-03437), the Olle Engkvist Foundation (grant number 200-575), the project grant "Probing charge- and mass- transfer reactions on the atomic level" (2018.0028) from the Knut and Alice Wallenberg Foundation, and the Swedish Foundation for International Collaboration in Research and Higher Education (STINT, grant number PT2017-7328 awarded to JNB and MHS). This work was performed at the Swedish National Infrastructure, DESIREE (Swedish Research Council Contracts No. 2017-00621 and 2021-00155). The authors also thank the DESIREE technical staff for their invaluable assistance during the whole experiment.

VI. REFERENCES

[1]B. Shukla, A. Susa, A. Miyoshi, and M. Koshi, J. Phys. Chem. A **112**, 2362–2369 (2008), pMID: 18298104.
[2]M. Agúndez and V. Wakelam, Chem. Rev. **113**, 8710–8737 (2013).
[3]A. Dalgarno and R. A. McCray, Astrophys. J. **181**, 95–100 (1973).
[4]E. Herbst, Nature **289**, 656–657 (1981).
[5]M. C. McCarthy, C. A. Gottlieb, H. Gupta, and P. Thaddeus, Astrophys. J. **652**, L141–L144 (2006).
[6]Cernicharo, J., Guélin, M., Agúndez, M., Kawaguchi, K., McCarthy, M., and Thaddeus, P., Astro. Astrophys. **467**, L37–L40 (2007).
[7]S. Brünken, H. Gupta, C. A. Gottlieb, M. C. McCarthy, and P. Thaddeus, Astrophys. J. **664**, L43–L46 (2007).
[8]Agúndez, M., Cernicharo, J., Guélin, M., Kahane, C., Roueff, E., Klos, J., Aoiz, F. J., Lique, F., Marcelino, N., Goicoechea, J. R., González García, M., Gottlieb, C. A., McCarthy, M. C., and Thaddeus, P., Astro. Astrophys. **517**, L2 (2010).
[9]Cernicharo, J., Marcelino, N., Pardo, J. R., Agúndez, M., Tercero, B., de Vicente, P., Cabezas, C., and Bermúdez, C., Astro. Astrophys. **641**, L9 (2020).
[10]J. Cernicharo, M. Guélin, M. Agúndez, M. C. McCarthy, and P. Thaddeus, Astrophys. J. **688**, L83–L86 (2008).
[11]C. Walsh, N. Harada, E. Herbst, and T. J. Millar, Astrophys. J. **700**, 752–761 (2009).
[12]E. Herbst and Y. Osamura, Astrophys. J. **679**, 1670–1679 (2008).
[13]E. Roueff and E. Herbst, J. Phys.: Conf. Ser. **192**, 012008 (2009).
[14]T. J. Millar, C. Walsh, M. A. Cordiner, R. N. Chuimín, and E. Herbst, Astrophys. J. **662**, L87–L90 (2007).
[15]Cordiner, M. A. and Sarre, P. J., Astro. Astrophys. **472**, 537–545 (2007).
[16]Astrophys. J. **762**, 121 (2012).
[17]B. A. Laws, Z. D. Levey, T. W. Schmidt, and S. T. Gibson, J. Am. Chem. Soc. **143**, 18684–18692 (2021).
[18]R. D. Thomas, H. T. Schmidt, G. Andler, M. Björkhage, M. Blom, L. Brännholm, E. Bäckström, H. Danared, S. Das, N. Haag, P. Halldén, F. Hellberg, A. I. S. Holm, H. A. B. Johansson, A. Källberg, G. Källersjö, M. Larsson, S. Leontein, L. Liljeby, P. Löfgren, B. Malm, S. Mannervik, M. Masuda, D. Misra, A. Orbán, A. Paál, P. Reinhed, K.-G. Rensfelt,

S. Rosén, K. Schmidt, F. Seitz, A. Simonsson, J. Weimer, H. Zettergren, and H. Cederquist, Rev. Sci. Instrum. **82**, 065112 (2011).
[19]V. Chandrasekaran, B. Kafle, A. Prabhakaran, O. Heber, M. Rappaport, H. Rubinstein, D. Schwalm, Y. Toker, and D. Zajfman, J. Phys. Chem. Lett. **5**, 4078–4082 (2014).
[20]N. Kono, T. Furukawa, H. Tanuma, J. Matsumoto, H. Shiromaru, T. Azuma, K. Najafian, M. S. Pettersson, B. Dynefors, and K. Hansen, Phys. Chem. Chem. Phys. **17**, 24732–24737 (2015).
[21]M. Wolf, H. V. Kiefer, J. Langeland, L. H. Andersen, H. Zettergren, H. T. Schmidt, H. Cederquist, and M. H. Stockett, Astrophys. J. **832**, 24 (2016).
[22]G. Ito, T. Furukawa, H. Tanuma, J. Matsumoto, H. Shiromaru, T. Majima, M. Goto, T. Azuma, and K. Hansen, Phys. Rev. Lett. **112**, 183001 (2014).
[23]S. Iida, W. Hu, R. Zhang, P. Ferrari, K. Masuhara, H. Tanuma, H. Shiromaru, T. Azuma, and K. Hansen, Mon. Not. R. Astron. Soc. **514**, 844–851 (2022).
[24]J. N. Bull, M. S. Scholz, E. Carrascosa, M. K. Kristiansson, G. Eklund, N. Punnakayathil, N. de Ruette, H. Zettergren, H. T. Schmidt, H. Cederquist, and M. H. Stockett, J. Chem. Phys. **151**, 114304 (2019).
[25]H. T. Schmidt, R. D. Thomas, M. Gatchell, S. Rosén, P. Reinhed, P. Löfgren, L. Brännholm, M. Blom, M. Björkhage, E. Bäckström, J. D. Alexander, S. Leontein, D. Hanstorp, H. Zettergren, L. Liljeby, A. Källberg, A. Simonsson, F. Hellberg, S. Mannervik, M. Larsson, W. D. Geppert, K. G. Rensfelt, H. Danared, A. Paál, M. Masuda, P. Halldén, G. Andler, M. H. Stockett, T. Chen, G. Källersjö, J. Weimer, K. Hansen, H. Hartman, and H. Cederquist, Rev. Sci. Instrum. **84**, 055115 (2013).
[26]E. Bäckström, D. Hanstorp, O. M. Hole, M. Kaminska, R. F. Nascimento, M. Blom, M. Björkhage, A. Källberg, P. Löfgren, P. Reinhed, S. Rosén, A. Simonsson, R. D. Thomas, S. Mannervik, H. T. Schmidt, and H. Cederquist, Phys. Rev. Lett. **114**, 143003 (2015).
[27]N. Lopes and B. Ribeiro, "Non-negative matrix factorization (nmf)," in *Machine Learning for Adaptive Many-Core Machines - A Practical Approach* (Springer International Publishing, Cham, 2015) pp. 127–154.
[28]I. S. Dhillon and S. Sra, "Generalized nonnegative matrix approximations with bregman divergences," in *Neural Information Processing Systems (NIPS)* (2005).
[29]M. H. Stockett, M. Björkhage, H. Cederquist, H. T. Schmidt, and H. Zettergren, Faraday Discuss. **217**, 126–137 (2019).
[30]M. H. Stockett, M. Björkhage, H. Cederquist, H. T. Schmidt, and Z. Henning, Proceedings of the International Astronomical Union **15**, 127–131 (2019).
[31]E. P. Wigner, Phys. Rev. **73**, 1002–1009 (1948).
[32]J. W. Farley, Phys. Rev. A **40**, 6286–6292 (1989).
[33]M. H. Stockett, J. N. Bull, J. T. Buntine, E. Carrascosa, E. K. Anderson, M. Gatchell, M. Kaminska, R. F. Nascimento, H. Cederquist, H. T. Schmidt, and H. Zettergren, Eur. Phys. J. D **74** (2020).
[34]T. Beyer and D. F. Swinehart, Comm. ACM **16** (1973).
[35]T. H. Dunning, J. Chem. Phys. **90**, 1007–1023 (1989).
[36]M. J. Frisch, G. W. Trucks, H. B. Schlegel, G. E. Scuseria, M. A. Robb, J. R. Cheeseman, G. Scalmani, V. Barone, G. A. Petersson, H. Nakatsuji, X. Li, M. Caricato, A. V. Marenich, J. Bloino, B. G. Janesko, R. Gomperts, B. Mennucci, H. P. Hratchian, J. V. Ortiz, A. F. Izmaylov, J. L. Sonnenberg, D. Williams-Young, F. Ding, F. Lipparini, F. Egidi, J. Goings, B. Peng, A. Petrone, T. Henderson, D. Ranasinghe, V. G. Zakrzewski, J. Gao, N. Rega, G. Zheng, W. Liang, M. Hada, M. Ehara, K. Toyota, R. Fukuda, J. Hasegawa, M. Ishida, T. Nakajima, Y. Honda, O. Kitao, H. Nakai, T. Vreven, K. Throssell, J. A. Montgomery, Jr., J. E. Peralta, F. Ogliaro, M. J. Bearpark, J. J. Heyd, E. N. Brothers, K. N. Kudin, V. N. Staroverov, T. A. Keith, R. Kobayashi, J. Normand, K. Raghavachari, A. P. Rendell, J. C. Burant, S. S. Iyengar, J. Tomasi, M. Cossi, J. M. Millam, M. Klene, C. Adamo, R. Cammi, J. W. Ochterski, R. L. Martin, K. Morokuma, O. Farkas, J. B. Foresman, and D. J. Fox, "Gaussian~16 Revision C.01," (2016), gaussian Inc. Wallingford CT.
[37]J. Zhou, E. Garand, and D. M. Neumark, J. Chem. Phys. **127**, 154320 (2007).
[38]E. E. Etim, P. Gorai, A. Das, S. K. Chakrabarti, and E. Arunan, Astrophys. J. **832**, 144 (2016).
[39]T. R. Taylor, C. Xu, and D. M. Neumark, J. Chem. Phys. **108**, 10018–10026 (1998).
[40]James N. Bull, et al. (unpublished data).
[41]J. Gregory, J. R. R. Verlet, and J. N. Bull, Phys. Chem. Chem. Phys. **22**, 8284–8288 (2020).
[42]T. Pino, M. Tulej, F. Güthe, M. Pachkov, and J. P. Maier, J. Chem. Phys. **116**, 6126–6131 (2002).
[43]K. D. Jordan and F. Wang, "Theory of dipole-bound anions," Annual Review of Physical Chemistry **54**, 367–396 (2003), pMID: 12626734, https://doi.org/10.1146/annurev.physchem.54.011002.103851.
[44]H. T. Schmidt, G. Eklund, K. C. Chartkunchand, E. K. Anderson, M. Kamińska, N. de Ruette, R. D. Thomas, M. K. Kristiansson, M. Gatchell, P. Reinhed, S. Rosén, A. Simonsson, A. Källberg, P. Löfgren, S. Mannervik, H. Zettergren, and H. Cederquist, Phys. Rev. Lett. **119**, 073001 (2017).
[45]N. Sakai, T. Sakai, Y. Osamura, and S. Yamamoto, Astrophys. J. **667**, L65–L68 (2007).

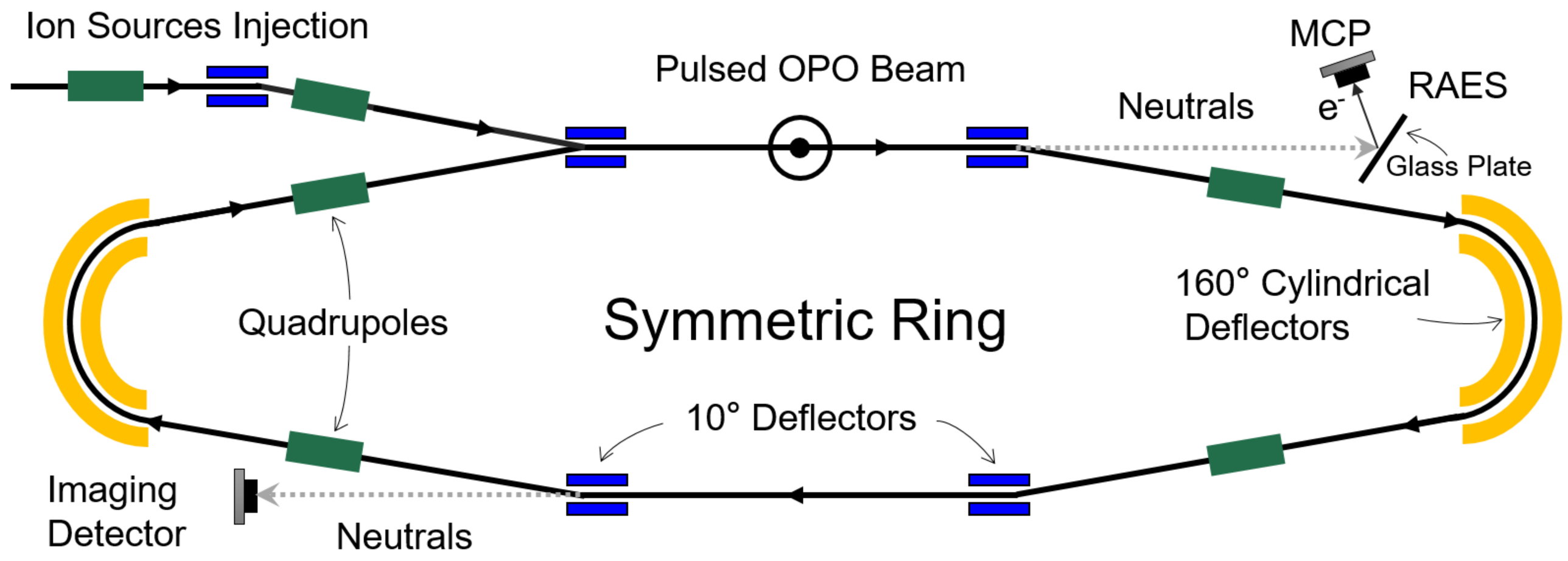
Ion Sources Injection
Pulsed OPO Beam
MCP
RAES
Neutrals
e-
Glass Plate
Quadrupoles
Symmetric Ring
160° Cylindrical
Deflectors
10° Deflectors
Imaging
Detector
Neutrals

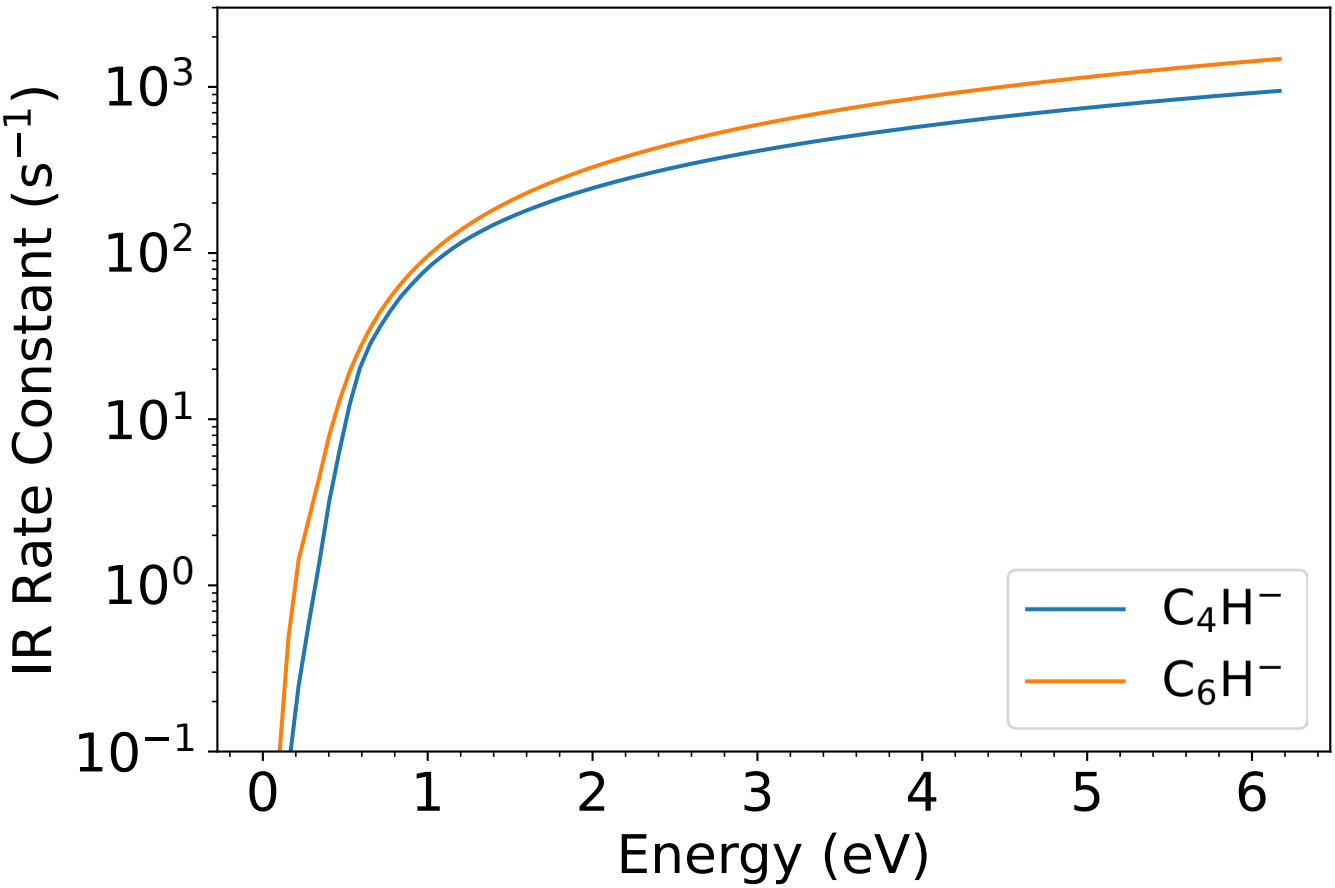
IR Rate Constant (s^{-1})
10^3
10^2
10^1
10^0
10^{-1}
0
1
2
3
4
5
6
Energy (eV)
C_4H^-
C_6H^-

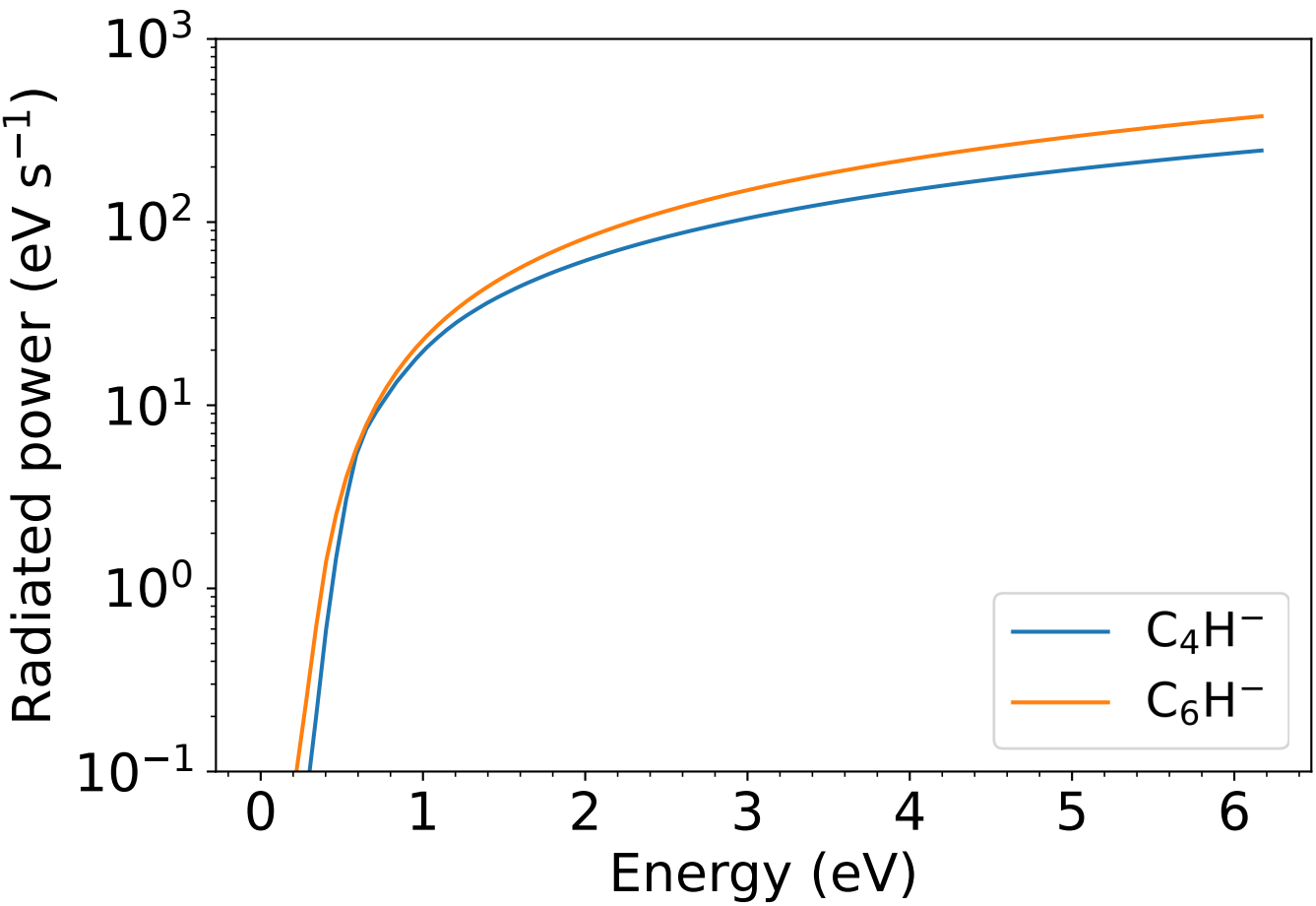
Radiated power (eV s^{-1})
10^3
10^2
10^1
10^0
10^{-1}
0
1
2
3
4
5
6
Energy (eV)
C_4H^-
C_6H^-

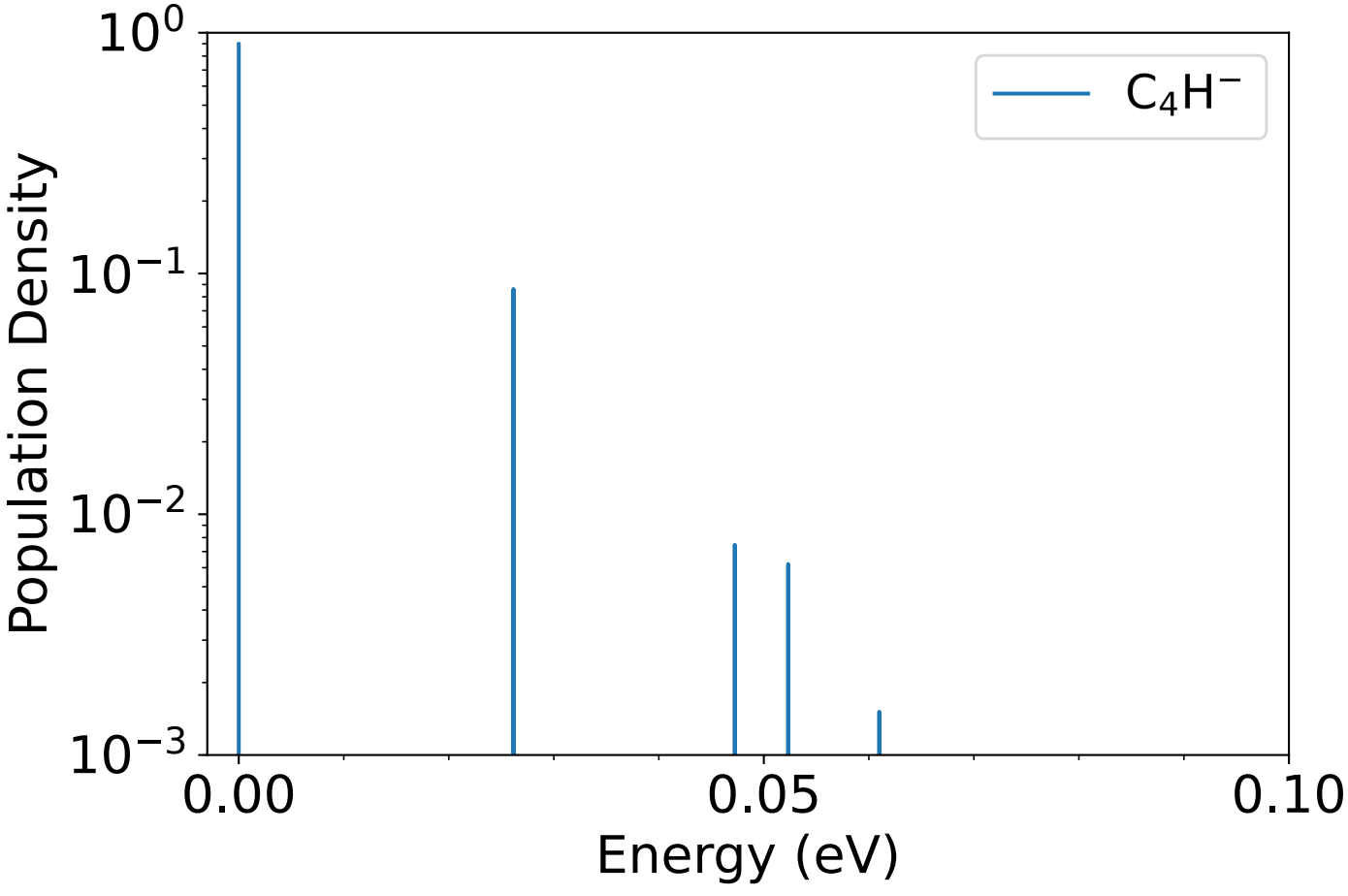
10^0
10^{-1}
10^{-2}
10^{-3}
Population Density
C_4H^-
0.00
0.05
0.10
Energy (eV)

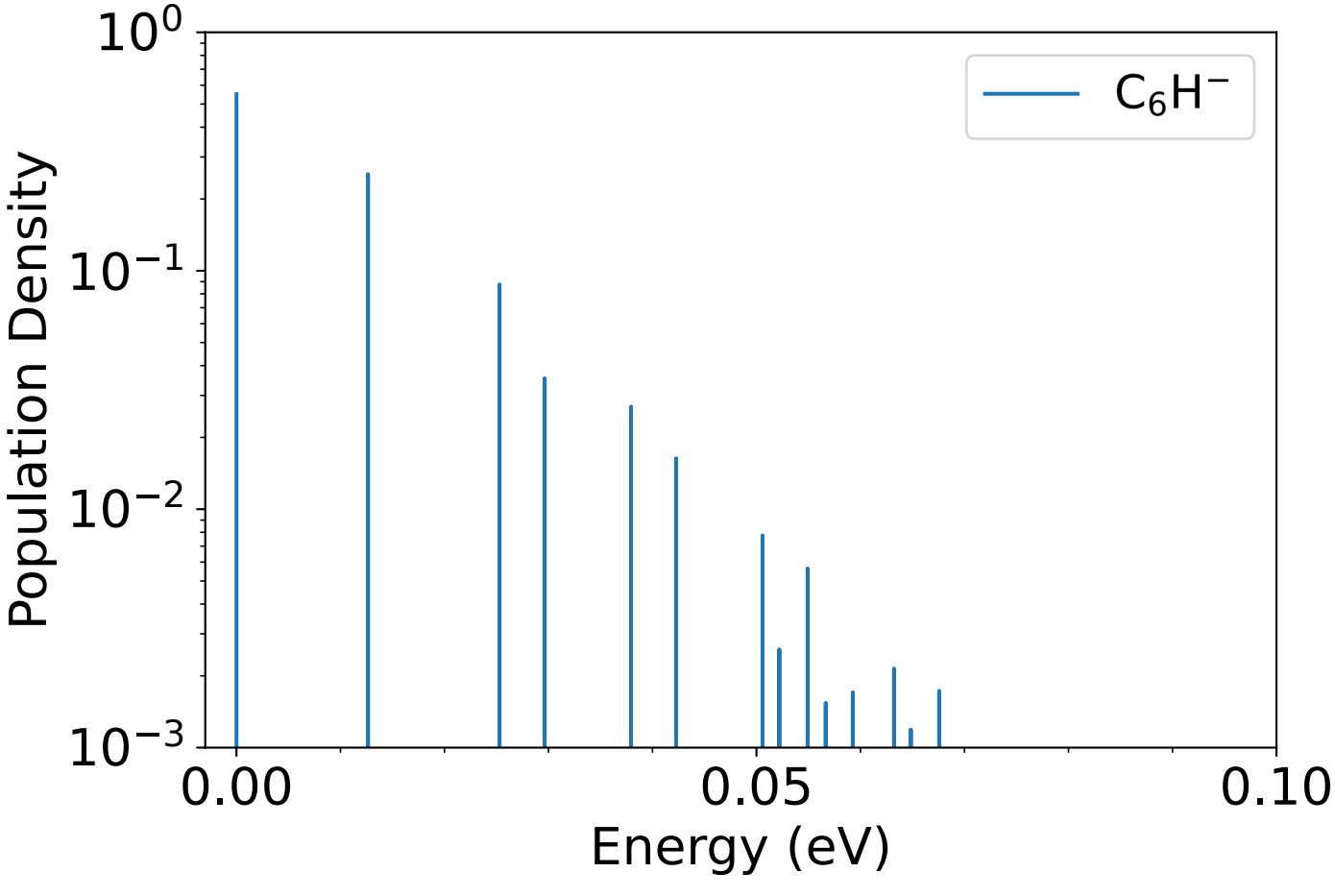
10^0
10^{-1}
10^{-2}
10^{-3}
Population Density
C_6H^-
0.00
0.05
0.10
Energy (eV)

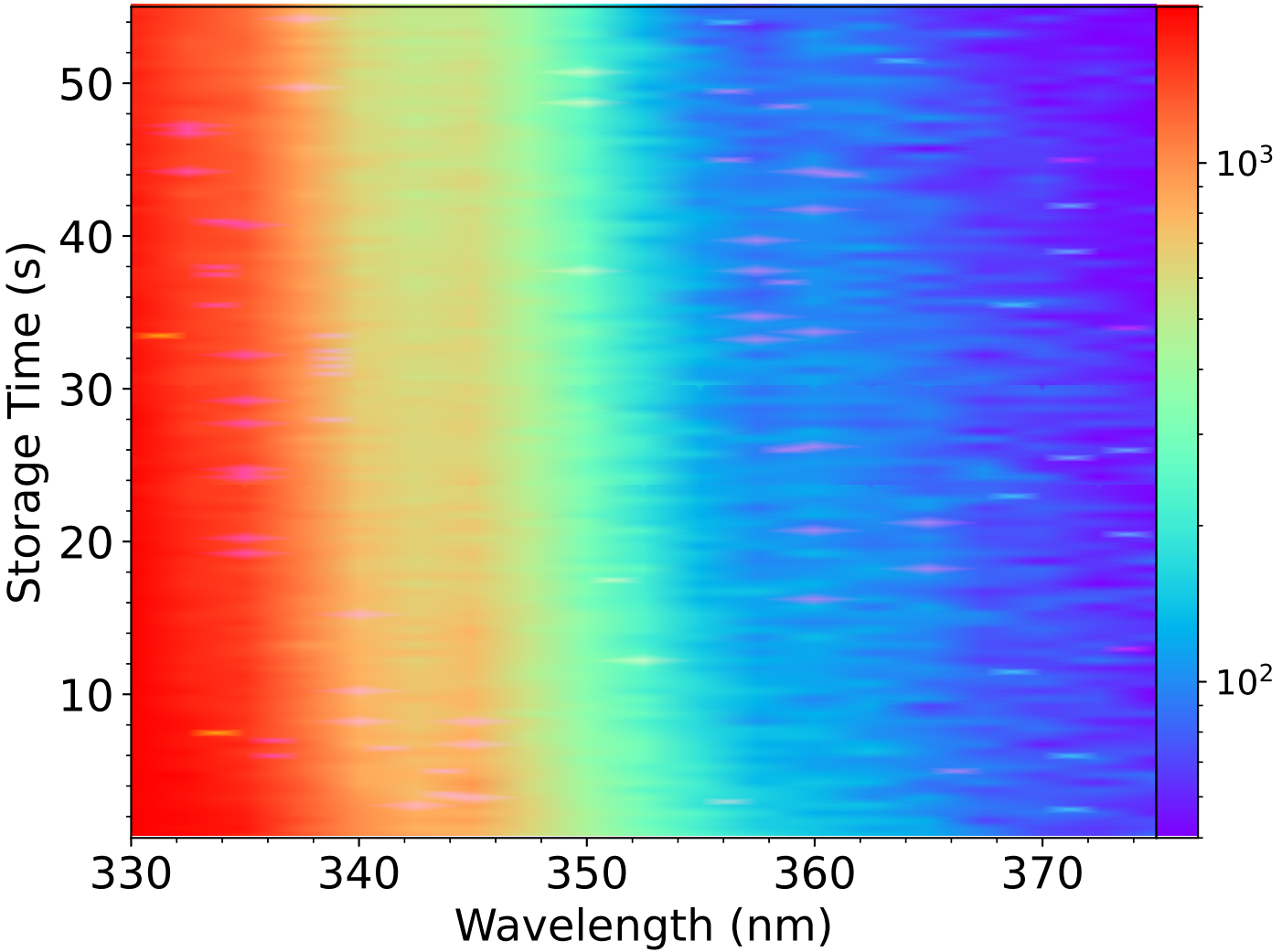
Storage Time (s)
50
40
30
20
10
330
340
350
360
370
Wavelength (nm)
10^3
10^2

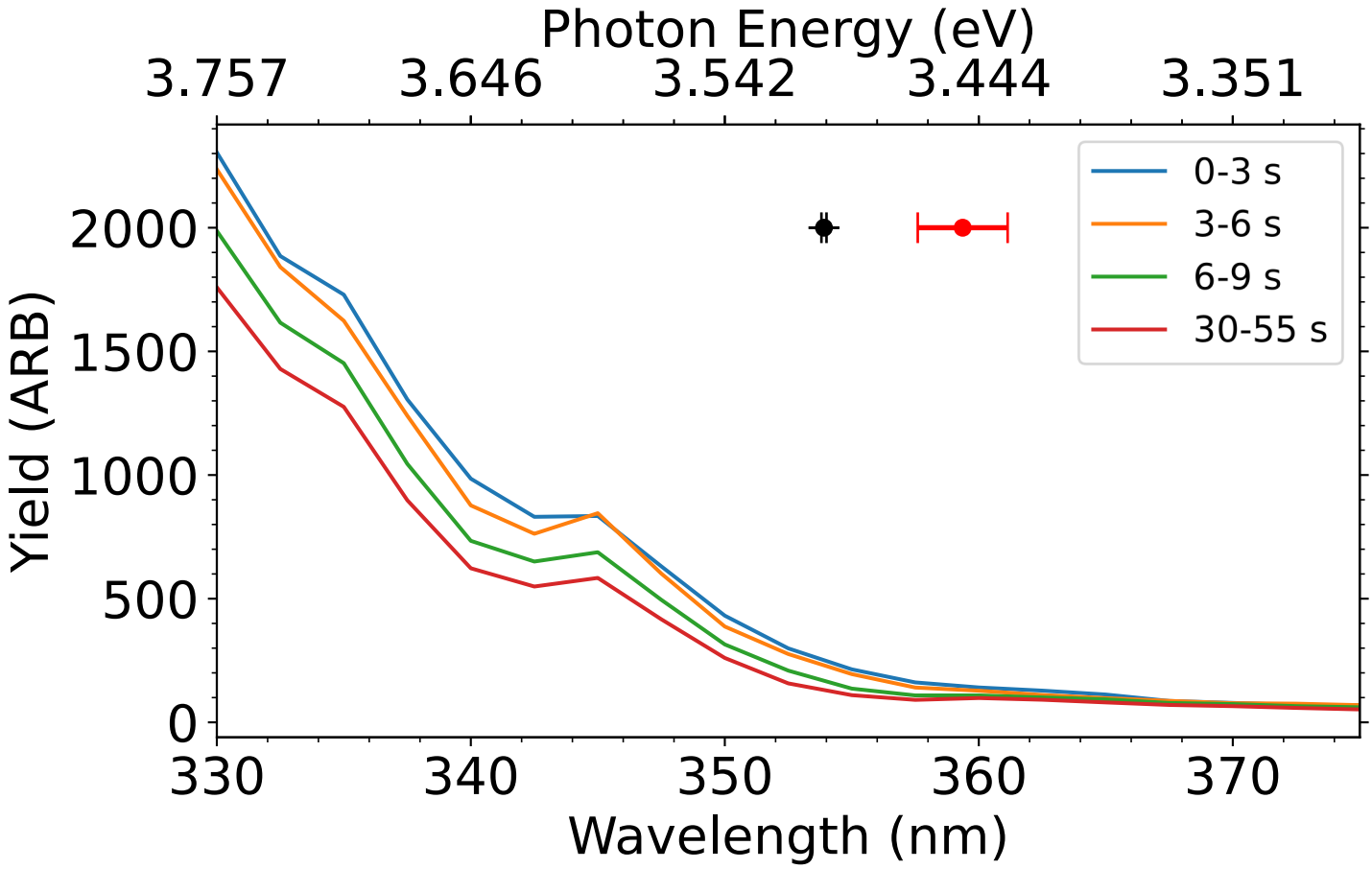
Photon Energy (eV)
3.757
3.646
3.542
3.444
3.351
Yield (ARB)
2000
1500
1000
500
0
0-3 s
3-6 s
6-9 s
30-55 s
330
340
350
360
370
Wavelength (nm)

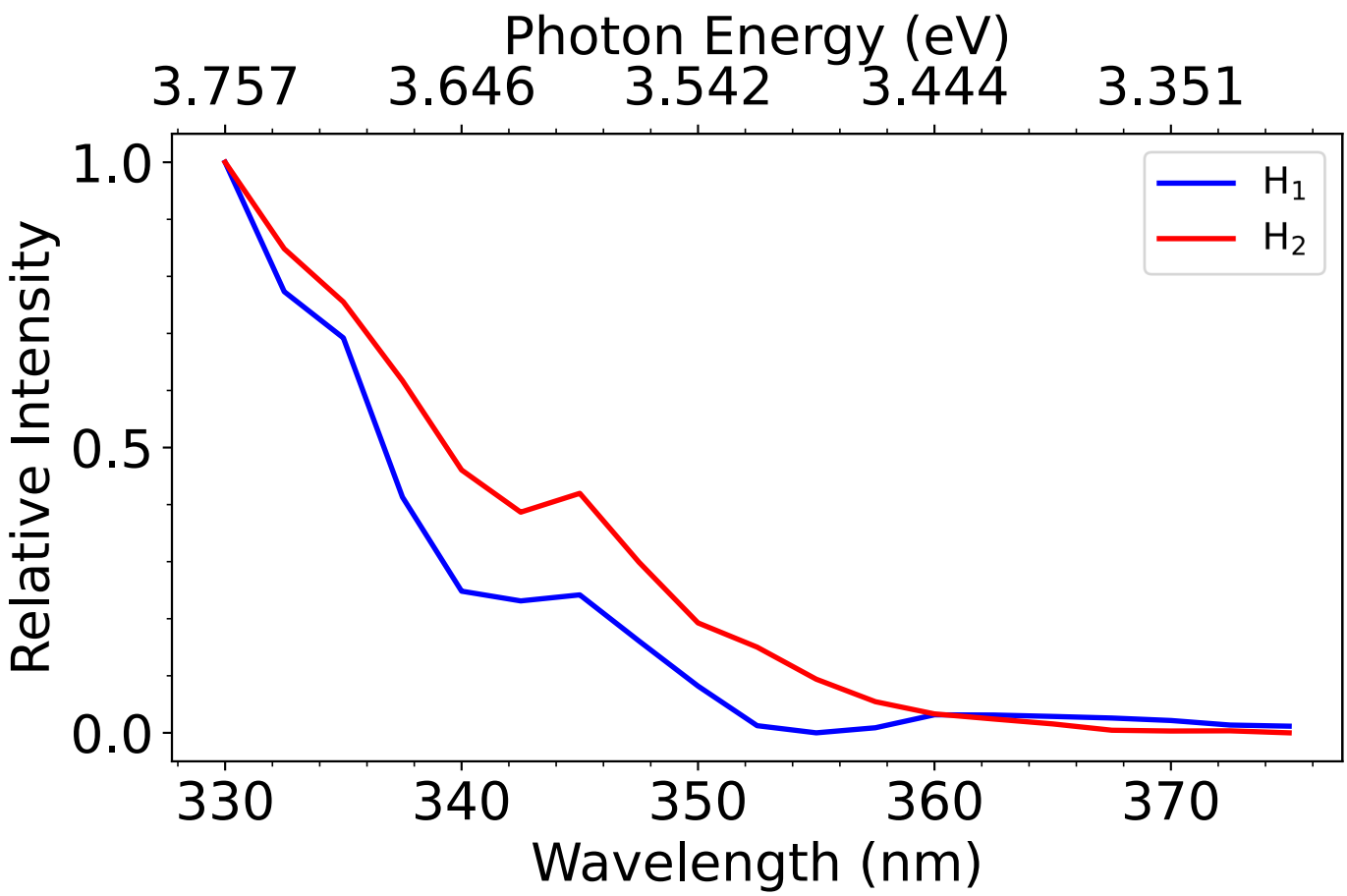
Photon Energy (eV)
3.757
3.646
3.542
3.444
3.351
Relative Intensity
1.0
0.5
0.0
H1
H2
330
340
350
360
370
Wavelength (nm)

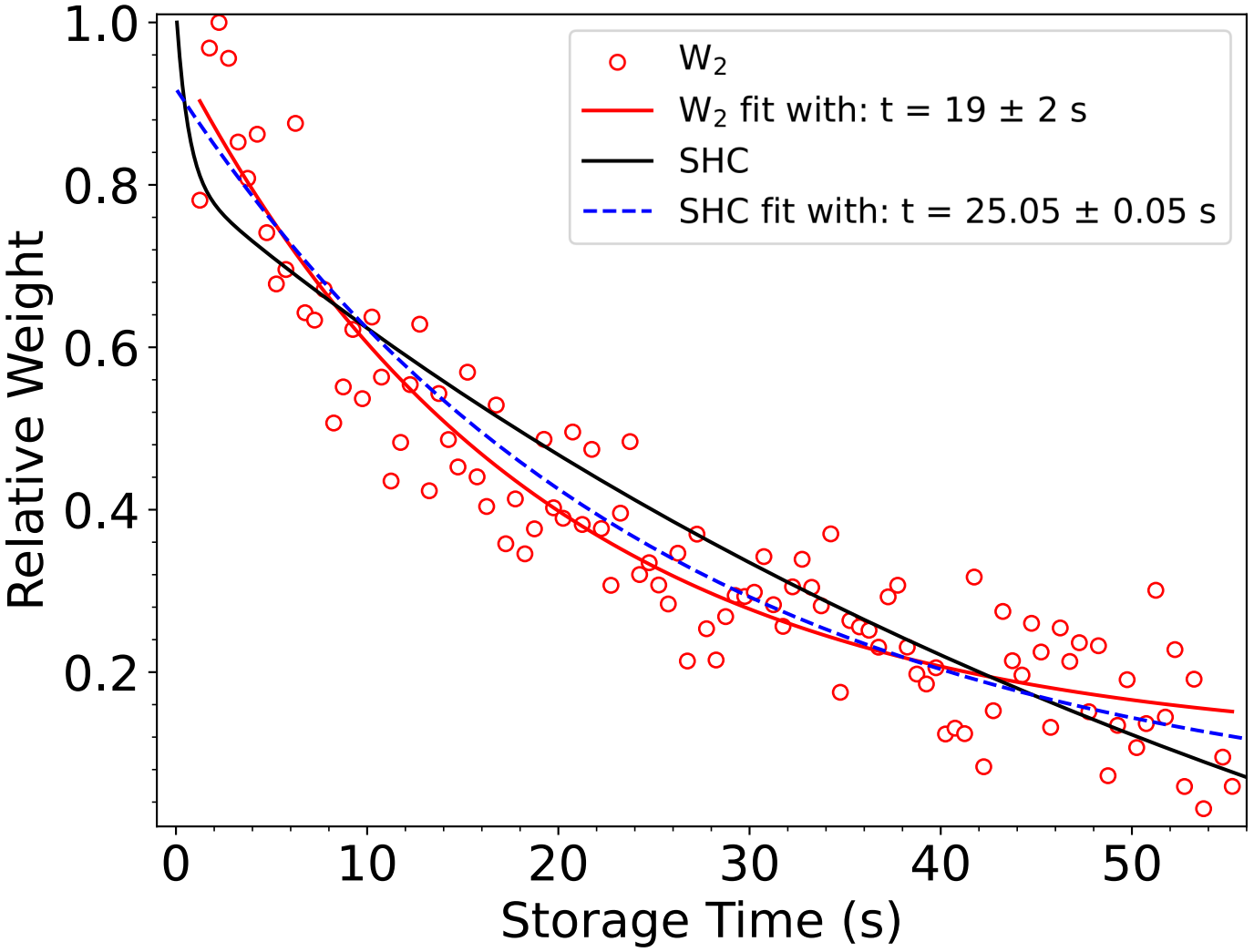
1.0
0.8
0.6
0.4
0.2
Relative Weight
0
10
20
30
40
50
Storage Time (s)
W2
W2 fit with: t = 19 ± 2 s
SHC
SHC fit with: t = 25.05 ± 0.05 s

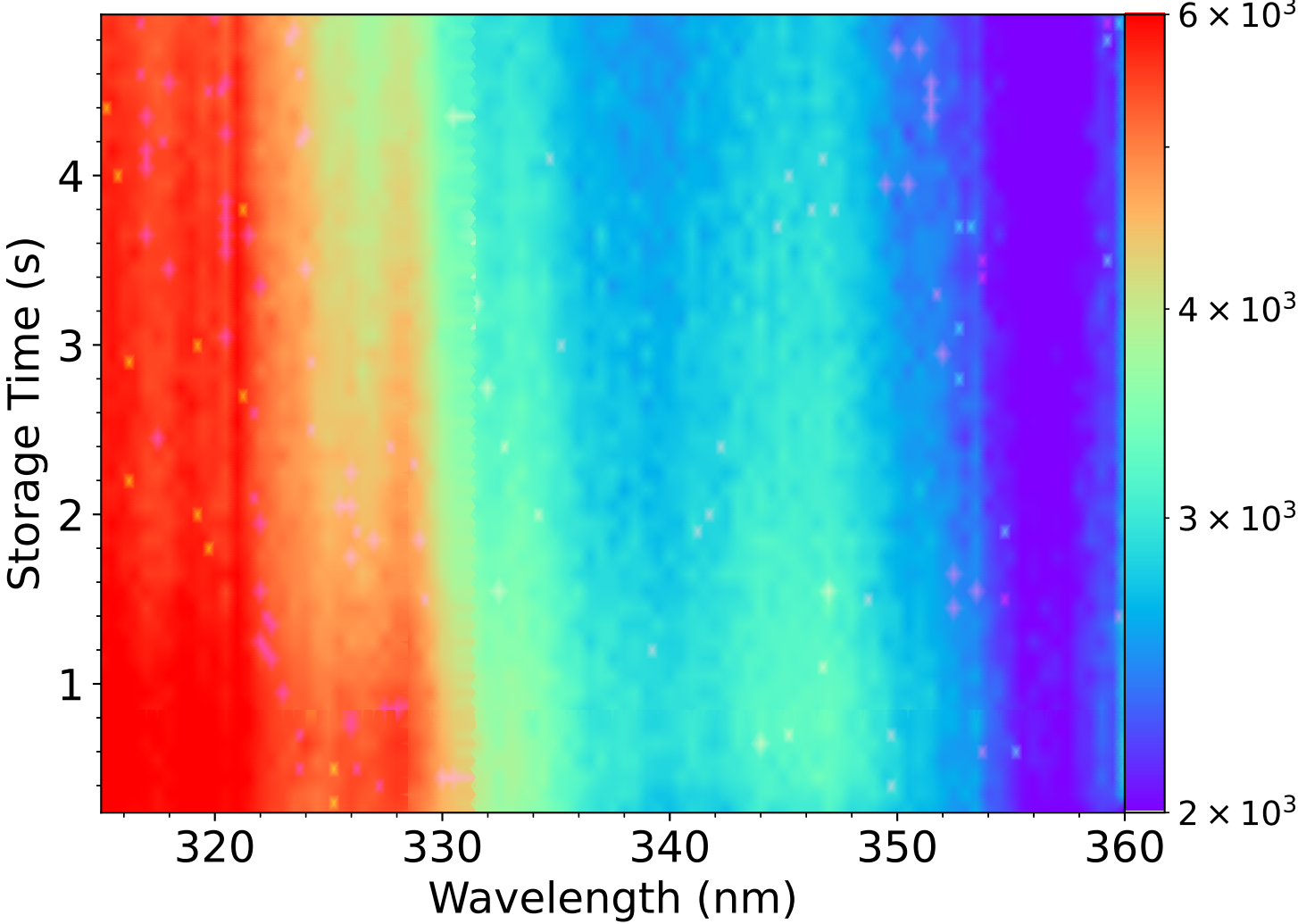
Storage Time (s)
1
2
3
4
320
330
340
350
360
Wavelength (nm)
6 × 10^3
4 × 10^3
3 × 10^3
2 × 10^3

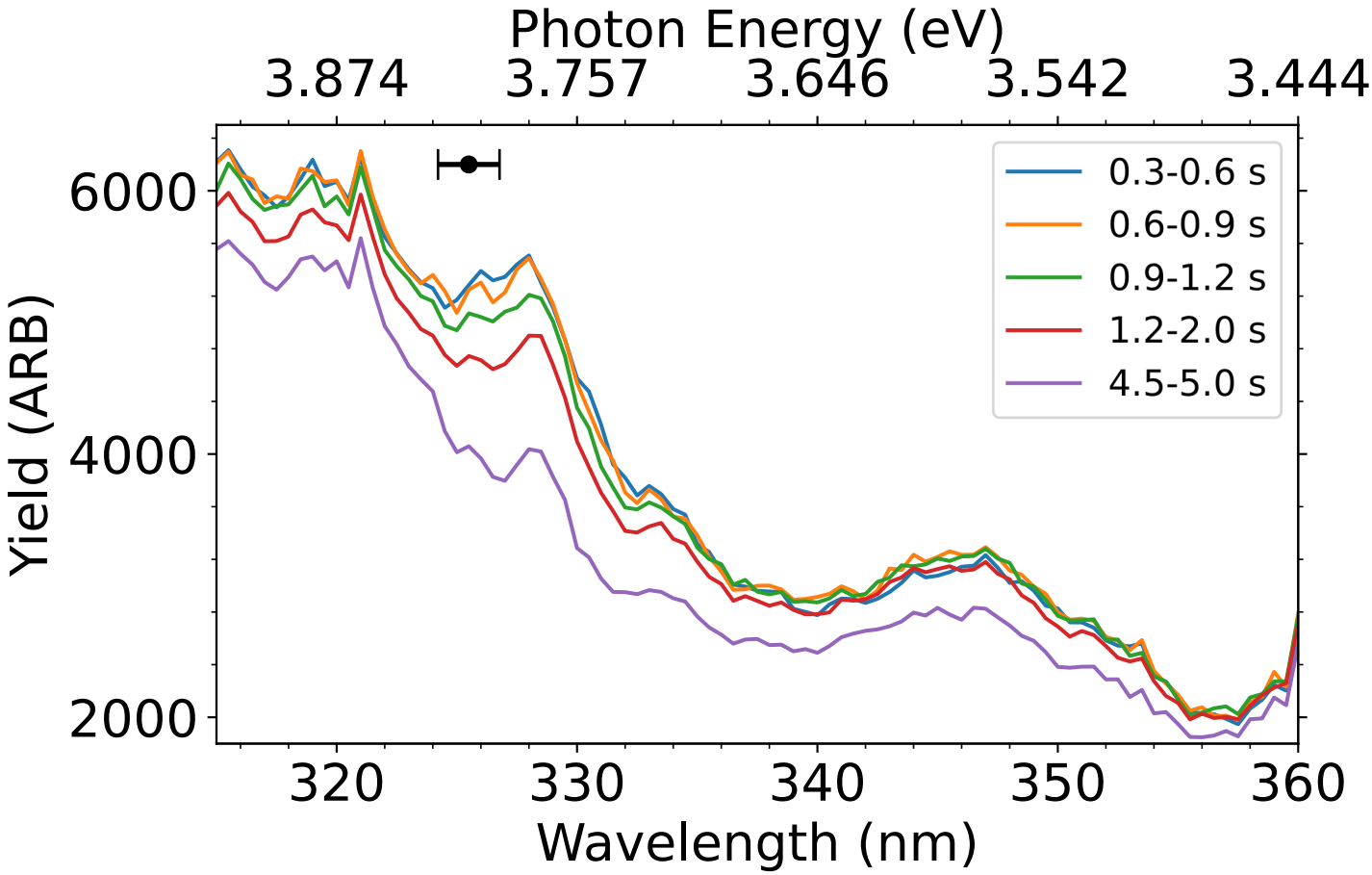
Photon Energy (eV)
3.874
3.757
3.646
3.542
3.444
6000
4000
2000
Yield (ARB)
0.3-0.6 s
0.6-0.9 s
0.9-1.2 s
1.2-2.0 s
4.5-5.0 s
320
330
340
350
360
Wavelength (nm)

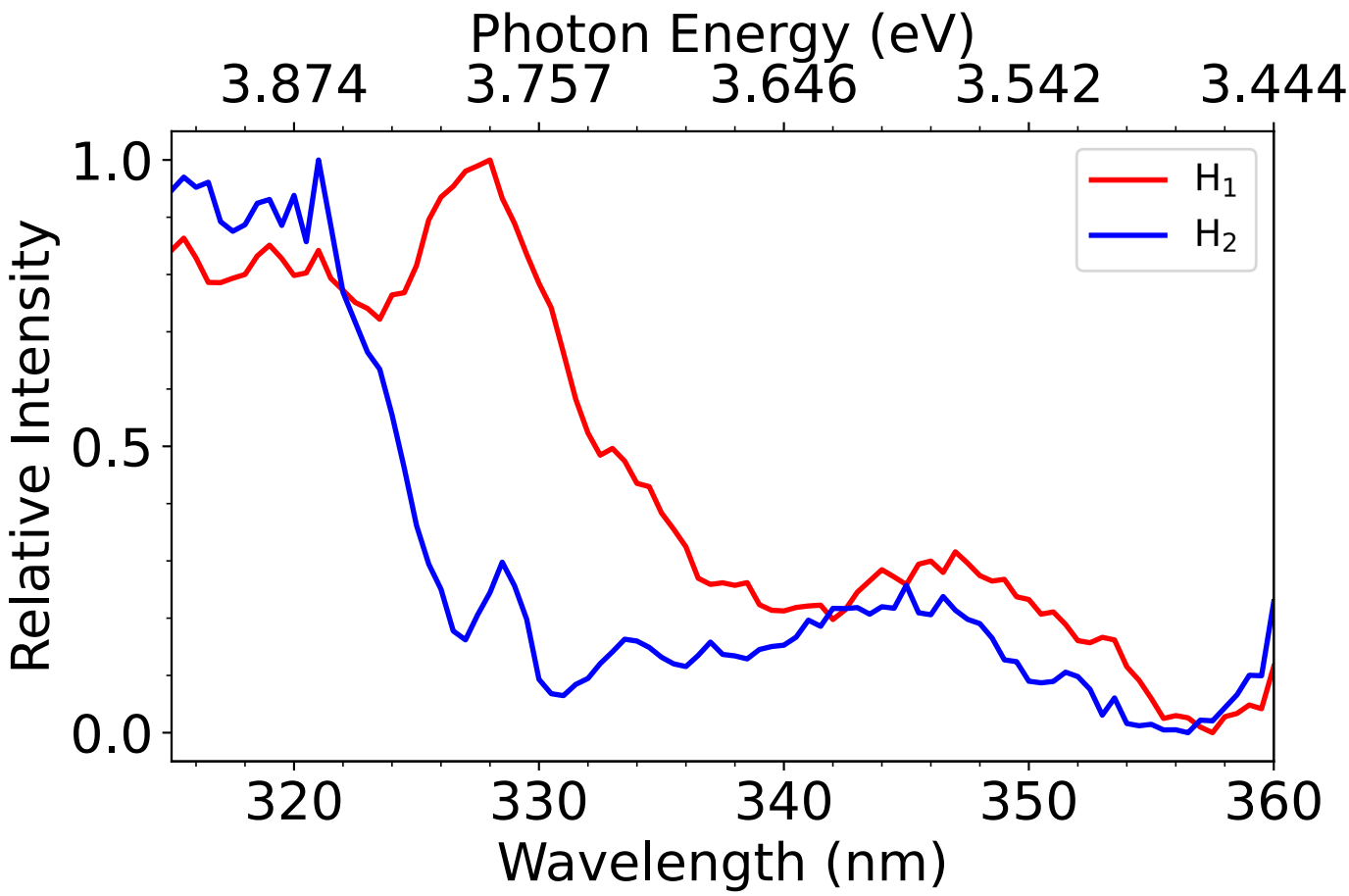
Photon Energy (eV)
3.874
3.757
3.646
3.542
3.444
1.0
0.5
0.0
Relative Intensity
H1
H2
320
330
340
350
360
Wavelength (nm)

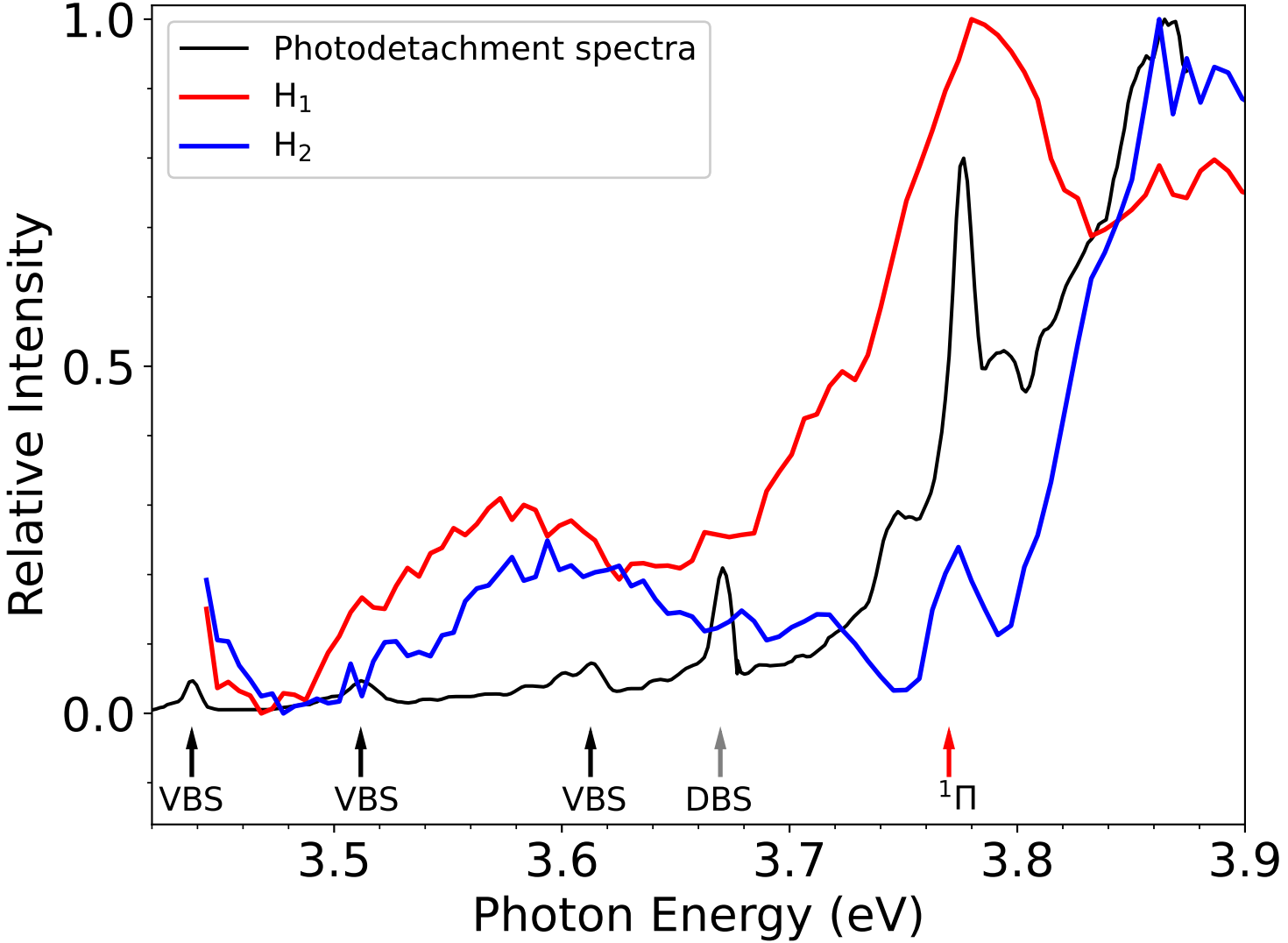
Photodetachment spectra
H1
H2
Relative Intensity
1.0
0.5
0.0
VBS
VBS
VBS
DBS
1Π
3.5
3.6
3.7
3.8
3.9
Photon Energy (eV)

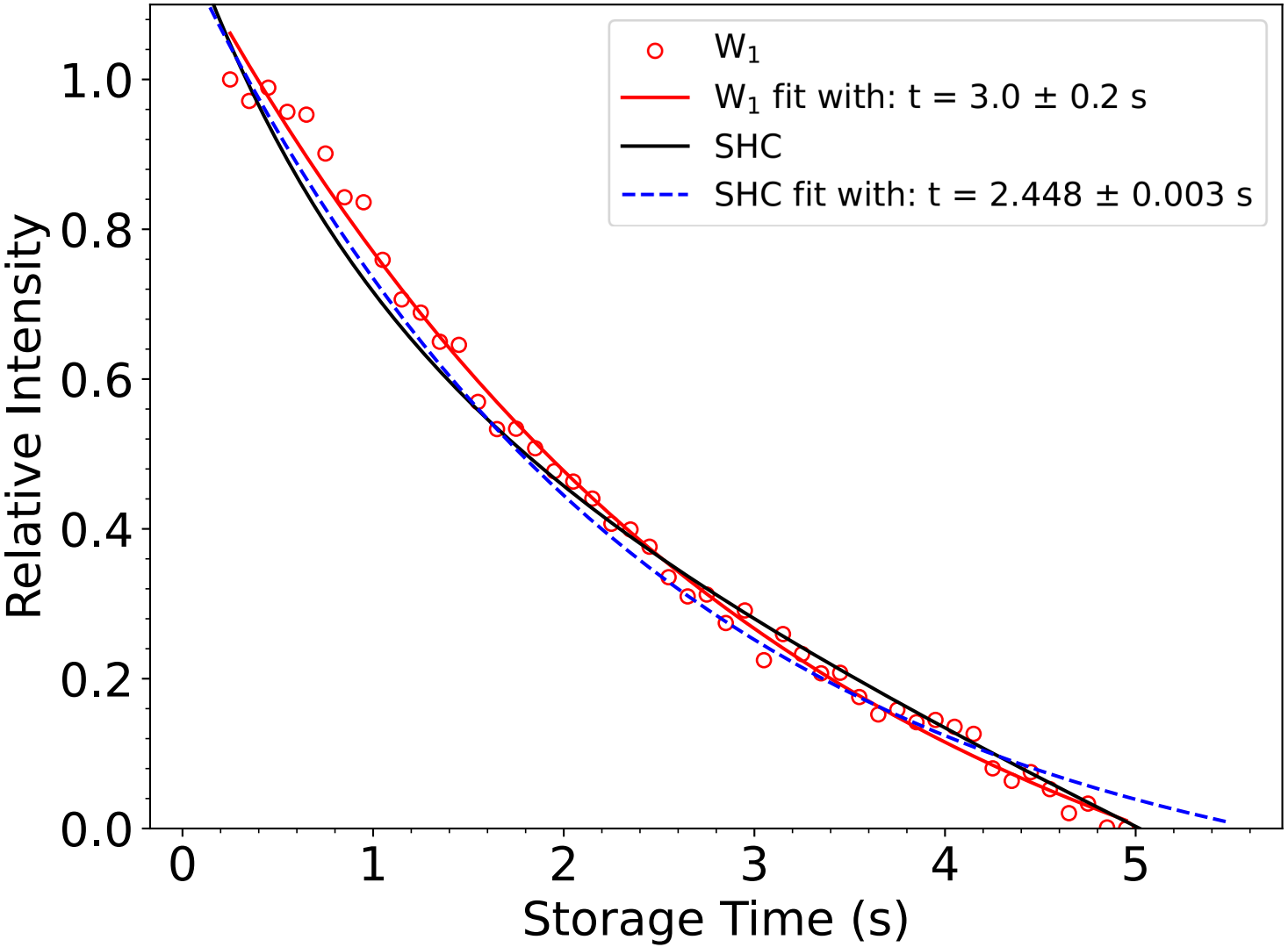
W1
W1 fit with: t = 3.0 ± 0.2 s
SHC
SHC fit with: t = 2.448 ± 0.003 s
Relative Intensity
Storage Time (s)
0.0
0.2
0.4
0.6
0.8
1.0
0
1
2
3
4
5